This is an open access article published under an ACS AuthorChoice License, which permits copying and redistribution of the article or any adaptations for non-commercial purposes.

JACS
JOURNAL OF THE AMERICAN CHEMICAL SOCIETY
Article
pubs.acs.org/JACS

Kinetic Study of Hydrogen Evolution Reaction over Strained MoS_2 with Sulfur Vacancies Using Scanning Electrochemical Microscopy

Hong Li,[†,¶] Minshu Du,[∥,¶] Michal J. Mleczko,[‡] Ai Leen Koh,[§] Yoshio Nishi,[‡] Eric Pop,[‡,⊥] Allen J. Bard,[*,∥] and Xiaolin Zheng[*,†]

[†]Department of Mechanical Engineering, [‡]Department of Electrical Engineering, [§]Stanford Nano Shared Facilities, and [⊥]Precourt Institute for Energy, Stanford University, Stanford, California 94305, United States

[∥]Center for Electrochemistry, Department of Chemistry, The University of Texas at Austin, Austin, Texas 78712, United States

Supporting Information

ABSTRACT: Molybdenum disulfide (MoS_2), with its active edge sites, is a proposed alternative to platinum for catalyzing the hydrogen evolution reaction (HER). Recently, the inert basal plane of MoS_2 was successfully activated and optimized with excellent intrinsic HER activity by creating and further straining sulfur (S) vacancies. Nevertheless, little is known about the HER kinetics of those S vacancies and the additional effects from elastic tensile strain. Herein, scanning electrochemical microscopy was used to determine the HER kinetic data for both unstrained S vacancies (formal potential $E_v^0 = -0.53\ V_{Ag/AgCl}$, electron-transfer coefficient $\alpha_v = 0.4$, electron-transfer rate constant $k_v^0 = 2.3 \times 10^{-4}$ cm/s) and strained S vacancies ($E_{sv}^0 = -0.53\ V_{Ag/AgCl}$, $\alpha_{sv} = 0.4$, $k_{sv}^0 = 1.0 \times 10^{-3}$ cm/s) on the basal plane of MoS_2 monolayers, and the strained S vacancy has an electron-transfer rate 4 times higher than that of the unstrained S vacancy. This study provides a general platform for measuring the kinetics of two-dimensional material-based catalysts.

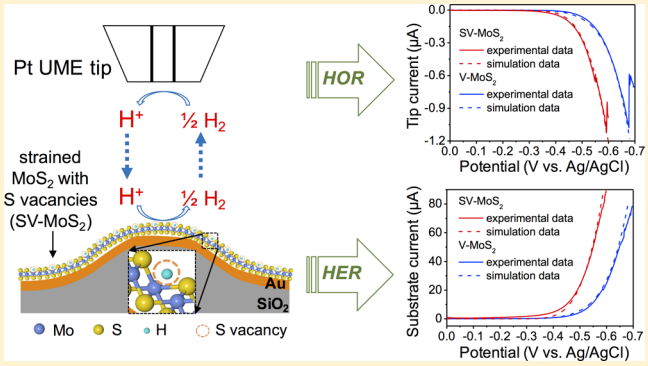

INTRODUCTION

Molybdenum disulfide (MoS_2) has been extensively studied as an attractive catalyst for the hydrogen evolution reaction (HER) for about three decades.[1−4] The edge sites of MoS_2 were first theoretically proposed as active sites in 2005[5] and then were experimentally confirmed in 2007.[6] Since then, efforts to optimize MoS_2 for HER have focused on maximizing the density of edge sites.[7−9] Very recently, the basal plane of MoS_2, which is long thought to be inert for HER, was successfully activated by creating sulfur (S) vacancies that generated new gap states near the Fermi level for hydrogen binding[10,11] and further enhanced by elastically straining the S vacancies that moved the new gap states closer to the Fermi level.[11] So far, all the understanding of the HER activity of those unstrained or strained S vacancies comes from thermodynamic consideration of their hydrogen adsorption energy,[11] and little is known about the kinetics of those S vacancies on the basal plane of MoS_2.

In this report, we employ scanning electrochemical microscopy (SECM)[12] equipped with a platinum (Pt) ultramicroelectrode (UME) to determine the kinetic information on both unstrained and strained S vacancies on the basal plane of MoS_2 monolayers. SECM has been previously applied to study the HER kinetics of metallic catalysts, such as Pt UME,[13] manganese (Mn) electrodes,[14] Pt and gold (Au) thin layer cells,[15] and metal nanoparticles.[16−18] These studies successfully determined the apparent rate constants and electron-transfer coefficients of the HER on Pt, palladium (Pd), and Mn electrodes.[13,14,16,17] More importantly, these studies established the methodology to quantify the HER kinetics, including simplifying the HER to be a quasi-reversible one-step reaction, using a thin layer cell formalism of the HER in the SECM theoretical equations[19] and describing the rates of the elementary steps and coverage of adsorbed hydrogen atoms on metallic electrodes based on the Volmer−Heyrovsky−Tafel mechanism.[15] Herein, we leverage the existing framework of the HER study (using SECM to investigate heterogeneous electrochemical reactions in the energy materials)[20−22] and adapt it to study the HER kinetics of the two-dimensional (2-D) catalyst of MoS_2 monolayers.

EXPERIMENTAL SECTION

Sample Fabrication. Continuous 2*H*-MoS_2 monolayers were grown in a homemade tube furnace.[11] The as-grown MoS_2 monolayers were transferred onto a silicon dioxide (SiO_2) substrate capped by a gold (90 nm)/titanium (10 nm) film using the poly(methyl methacrylate) (PMMA)-assisted transfer process. Briefly, a PMMA film was coated onto the as-grown MoS_2 on a SiO_2 substrate. Then the sample was soaked in potassium hydroxide solution to etch the surface

Received: February 5, 2016
Published: March 19, 2016

 © 2016 American Chemical Society
DOI: 10.1021/jacs.6b01377
J. Am. Chem. Soc. 2016, 138, 5123−5129

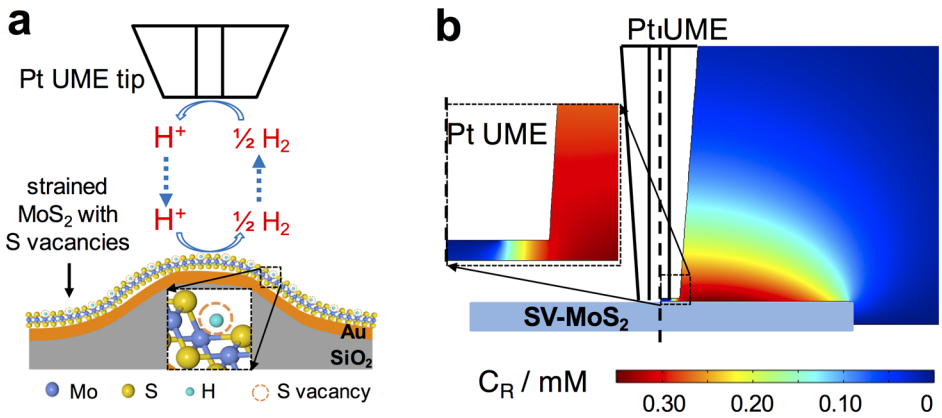

Figure 1. Methodology for quantifying the HER kinetics of strained/unstrained S vacancies on the basal plane of MoS_2 monolayers. (a) Schematic of the SECM measurement setup that operates in the SG−TC mode. The top trapezoid represents a Pt UME tip, and the bottom strained MoS_2 monolayer with S vacancies functions as the working electrode. H_2 is generated at the MoS_2 substrate through HER and subsequently collected and oxidized at the Pt UME tip through HOR. (b) Schematic of the complementary COMSOL simulation for the spatial distribution of hydrogen concentration (C_R/mM). The left side shows the tip and substrate 2-D configuration used in the simulation. The tip is a 25 μm diameter Pt wire in a glass shell (the ratio of glass to metal radius RG = 2). The SV-MoS_2 substrate has a diameter of about 0.5 mm. The right side shows a representative calculated C_R distribution (condition: SV-MoS_2 potential at −0.6 V and Pt UME tip potential at 0 V in 0.1 M $HClO_4$). Left inset: zoomed-in view of C_R near the tip−substrate gap. Bottom inset: color bar of C_R.

SiO_2 layer and to lift off the PMMA/MoS_2 bilayer film (see Supporting Note 1 for more details). Afterward, the PMMA/MoS_2 bilayer film was cleaned and floated on a deionized water surface and then scooped by the target substrate. In the center of the SiO_2 substrate, an array of SiO_2 nanopillars (Supporting Information) was obtained via dry etching of the SiO_2 film with an electron-beam resist as the etching mask, which was patterned by electron-beam lithography. Columns were defined with a negative-tone electron-beam resist (MaN-2403). The pitch size was 650 nm, and the diameter and height of the nanopillars were 350 and 80 nm, respectively. The gold nanopillars were formed after metallization of SiO_2 nanopillars. After thorough PMMA removal by sequential soaking of samples in acetone (60 °C for 10 min) and chloroform (60 °C for 1 h), the sample was strained by capillary force (see Supporting Note 1).[23] To create S vacancies, the cleaned MoS_2 samples were exposed to a cold and mild argon plasma (Supporting Note 1).[24] The MoS_2 film on the flat area of the substrate (outside the nanopillar array area) was used as MoS_2 with S vacancies (V-MoS_2), and that inside the nanopillar array area was used as strained MoS_2 with S vacancies (SV-MoS_2). The same PMMA-assisted transfer method was used to prepare the transmission electron microscopy (TEM) sample for S vacancy characterization by transferring the as-grown MoS_2 monolayers onto a TEM grid (quantifoil TEM grid, Ted Pella, Inc.), followed by PMMA removal through sequential acetone and chloroform soaking processes. Then the TEM sample was treated with mild Ar plasma to create S vacancies (Supporting Note 1).

Sample Characterization. Elastic strain in the sample was quantified from the well-established strain-Raman shift relation. Raman modes (E^1_{2g} and A_{1g}) of monolayer MoS_2 show red shifts upon uniaxial tensile strain with ratios of 2.2 and 0.5 cm^{-1}/% for E^1_{2g} and A_{1g} modes, respectively.[23,25] The magnitude of the elastic strain was thus calculated by the amount of red shifts of Raman modes (Figure S1). Aberration-corrected, monochromated TEM (ACTEM) imaging was performed using a FEI spherical aberration (Cs) image-corrected 80-300 Titan environmental (scanning) TEM operated at 80 kV under negative Cs imaging (NCSI) conditions,[26,27] wherein the spherical aberration coefficient of the objective lens was adjusted to approximately −15 μm, and images were acquired using a slight overfocus setting.

MoS_2 Working Electrode Preparation. The MoS_2 working electrodes were defined by masking the MoS_2 substrate using plastic tape with two hole openings. One hole was located on the unstrained MoS_2 area (V-MoS_2), and the other was on the nearby strained MoS_2 area (SV-MoS_2). Only the areas within the two holes were exposed to the electrolyte (Supporting Note 2 and Figure S2a).

Electrochemical Measurements. A 920C SECM (CH Instruments, Austin, TX) setup (Figure S2b) was employed for the electrochemical measurements. The MoS_2 samples on a Au/Ti-coated SiO_2/Si wafer were placed between an acrylic base and a PTFE cell with a 3.8 mm diameter orifice in the center. The samples were then connected to the potentiostat through a copper tape that was stuck to the bare Au part of the SiO_2/Si wafer. An O-ring with a 1.8 mm inner diameter was used to ensure a leakage-free connection. A 25 μm diameter Pt UME served as the tip, which was mounted facing downward to the substrate electrode. A Pt wire was used as a counter electrode, and a Ag/AgCl (1 M) electrode (CH Instruments, Austin, TX) acted as a reference electrode. All potentials shown in this work were relative to the Ag/AgCl (1 M) reference electrode unless stated otherwise. For the SECM experiments, a sealed glovebag was used to keep the system free of oxygen by purging with argon (Ar). All SECM measurements were performed in 0.1 M $HClO_4$ aqueous solution after deaeration via Ar bubbling.

The V-MoS_2 and SV-MoS_2 substrate electrodes were studied successively by being individually placed within the O-ring area. Two kinds of substrate generation−tip collection (SG−TC) modes were applied. First, the MoS_2 substrate potential was swept from 0 V to −0.7 V at a scan rate of 5 mV/s to generate hydrogen continuously, and the hydrogen was then collected at the Pt UME tip. Second, the MoS_2 substrate potential was switched between the open circuit potential (OCP) and the negative potentials for HER by dual-potential pulses. The pulse width was 0.5 s with five replicates. Also, the tip potential was held at 0 V as an amperometric sensor for collecting and oxidizing the hydrogen.

The measurements in Figure S6 were performed by a three-electrode electrochemical compression cell connected to a Gamry 600 potentiostat. The MoS_2 substrate served as the working electrode; A Pt wire acted as the counter electrode, and a Ag/AgCl electrode was used as the reference electrode. Sulfuric acid (0.3 M) with a pH value of 0.2 was used as the electrolyte.

Multiphysics Simulation. For SECM SG−TC experiments, numerical simulations were performed using COMSOL Multiphysics software v4.2 (COMSOL, Inc., Burlington, MA). A 2-D axial symmetry model was employed, where a 12.5 μm radius Pt UME (a = 12.5 μm, RG = 2) and a 250 μm radius MoS_2 substrate (b = 250 μm) were vertically aligned in a cylinder with a radius of 500 μm and a height of 500 μm. The distance between the tip and substrate was 5 μm for V-MoS_2 and 4 μm for SV-MoS_2 modeling. Since the scan rate

DOI: 10.1021/jacs.6b01377
J. Am. Chem. Soc. 2016, 138, 5123−5129

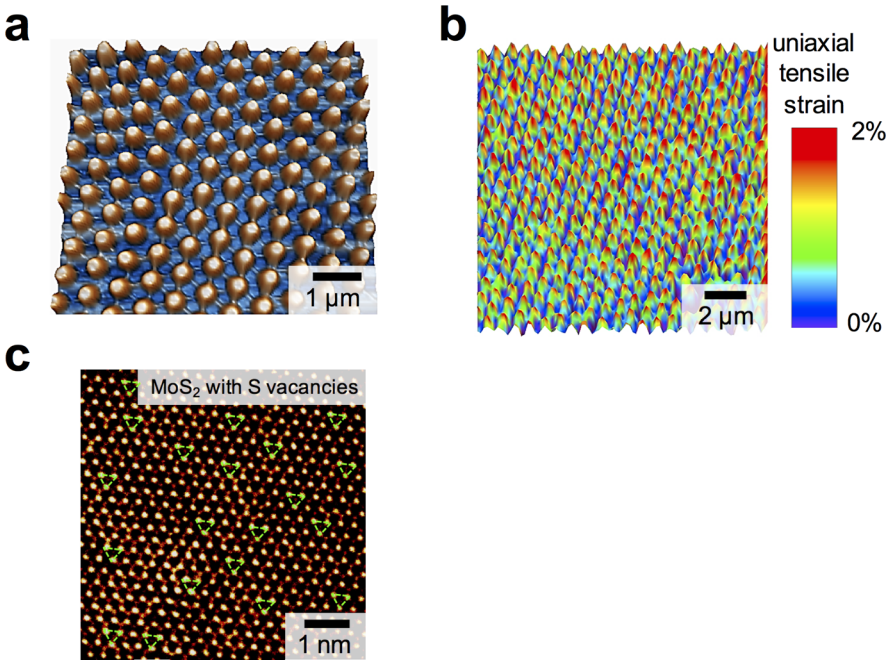

Figure 2. Quantification of the strain magnitude and S vacancy concentration in MoS_2 monolayers. (a) AFM image of a typical strained monolayer MoS_2 sample on patterned Au nanopillars. Scale bar is 1 μm. (b) Color-coded strain distribution in a strain-textured monolayer MoS_2 (14×14 μm^2) obtained from scanning micro-Raman spectroscopy. The peak strain magnitude on the top of nanopillars is about 2% (uniaxial tensile strain). (c) ACTEM image of a ~6.5×6.5 nm^2 MoS_2 monolayer with about ~13% S vacancies. The biggest and brightest dots are Mo atoms, and the small bright dots are S atoms. Small dim dots are mono-S vacancies, some of which have been labeled by dashed triangles. Scale bar is 1 nm.

of the SG−TC experiment was sufficiently slow (5 mV/s), we used the steady-state solver to perform the simulation for the potential sweep experiments. The kinetic parameters of the HER for V-MoS_2 and SV-MoS_2, including the formal potential E^0, electron-transfer coefficient α, and the rate constants k^0, were determined by finding the best fit between experimental and simulated linear sweep voltammograms for both the tip and the substrate (see Supporting Note 3 for more details).

■ RESULTS AND DISCUSSION

The SECM measurement setup is schematically illustrated in Figure 1a, and it operates in SG−TC mode.[28,29] The monolayer MoS_2 supported on Au is the substrate electrode (i.e., working electrode) that is negatively biased to evolve H_2 (i.e., HER: $H^+ + e^- \rightarrow \frac{1}{2}H_2$), while a Pt UME tip is held at constant 0 V vs Ag/AgCl (1 M) reference electrode and measures the current generated from the hydrogen oxidation reaction (i.e., HOR: $\frac{1}{2}H_2 \rightarrow H^+ + e^-$). Since the HOR current collected by the Pt UME tip is controlled by the diffusion of H_2 generated on the MoS_2 monolayer electrode, it excludes potential current contributions from other side reactions (e.g., reduction of growth precursor, molybdenum trioxide). As such, the SG−TC mode allows us to accurately determine the electron-transfer kinetics of the HER of the MoS_2 monolayer electrode. Complementary finite difference simulation is carried out to calculate the time-dependent concentration profiles of hydrogen and the proton in the SG−TC mode of SECM (Figure 1b). Since there is no recognized model for the HER kinetics of MoS_2, we assume that it follows a general one-electron-transfer reaction model with a Butler−Volmer formalism. All kinetic parameters were determined by identifying the best fit between the theoretically simulated and experimentally measured linear sweep voltammogram (LSV) curves. It is worth noting that the work described here concerns the relative rates of the HER reaction, thus the model selected to fit the data is of secondary importance.

For the SECM measurement, the working electrode consists of either unstrained (on flat substrates, V-MoS_2) or strained (on nanopillar arrays, Figure 1a shows a single nanopillar for a clear illustration, SV-MoS_2) MoS_2 monolayers with S vacancies. The atomic force microscopy (AFM) image in Figure 2a shows that the MoS_2 monolayers conformally and uniformly coat the nanopillar array. As such, MoS_2 monolayers are strained with larger strain on top of the nanopillars and smaller strain between nanopillars.[23] The magnitude and spatial distribution of the strain (Figure 2b) were determined by Raman spectroscopy,[25,30] and the peak strain magnitude is about 1% biaxial tensile strain, or equivalently 2% uniaxial tensile strain (see Figure S1). The S vacancies on the basal plane of MoS_2 monolayers are clearly shown in the ACTEM image (Figure 2c). In this image, the brightest spots correspond to Mo atoms and the lower intensity spots are the S atoms. The highlighted areas (dashed triangles) in Figure 2c correspond to the location of S atoms, but they exhibit dimmer or even absent brightness, indicating that one or two (top and bottom atomic planes) S atoms in the MoS_2 monolayer are missing. By counting the number of those S atoms with dimmer or absent brightness in the ACTEM image, we estimate that about 13% S atoms have been removed by the Ar plasma treatment.

Next, we ensure that the Pt UME tip is placed in the hydrogen diffusion layer above the MoS_2 working electrodes for the SECM measurements, so that the HOR current collected by the Pt UME tip is controlled by the diffusion of H_2 generated on the MoS_2 working electrodes. Specifically, the Pt UME tip was first electrochemically activated in Ar-saturated 0.1 M $HClO_4$ by cycling the applied potential between −0.2 and +1.0 V at a scan rate of 0.1 V/s for 20 cycles. Afterward, the Pt UME tip was held at a fixed potential at −0.35 V, where

DOI: 10.1021/jacs.6b01377
J. Am. Chem. Soc. 2016, 138, 5123−5129

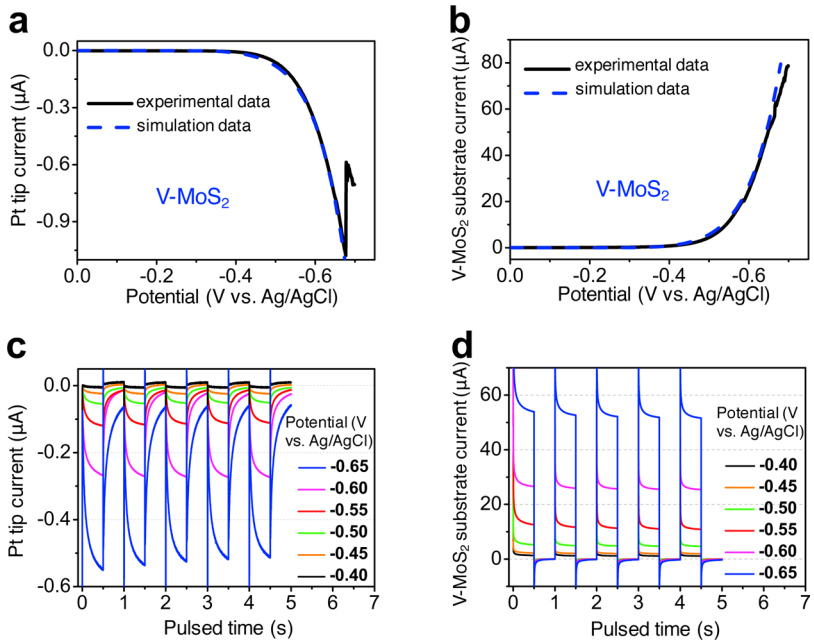

Figure 3. Experimental SECM measurement results of V-MoS_2 and the corresponding simulation results. (a) Pt tip and (b) V-MoS_2 substrate voltammograms in 0.1 M $HClO_4$ electrolyte and the corresponding simulation results (blue dashed lines). The separation between the tip and substrate electrode was ~5 μm. Tip potential was held at 0 V, and the substrate potential was swept from 0 V to −0.7 V at a scan rate of 5 mV/s. Transient and oscillating (c) Pt tip and (d) V-MoS_2 substrate current according to the double-pulse potential applied to the substrate. Tip potential was held at 0 V, and the substrate potential was switched between open circuit potential and the potentials listed in the legend to enable MoS_2 for HER. The pulse width was 0.5 s with five replicates.

proton reduction occurred, and the tip approached the MoS_2 substrate in the normal z direction using the "negative feedback mode",[31,32] while the MoS_2 substrate electrode was disconnected from the SECM (see Figure S2 for the setup). The tip approach curves for both V-MoS_2 and SV-MoS_2 samples were experimentally recorded and calculated with the negative feedback mode (Figure S3a,b). Excellent agreement between the measured and calculated tip approach curves confirms that the Pt tip approached the working substrate in the negative feedback mode as designed. As the Pt tip became closer to the MoS_2 substrate, its current decreased because the diffusion of the proton to the tip was hindered by the physical obstruction of the substrate.[33] When the Pt tip current drops to about 60% of its initial value ($I/I_\infty \approx 0.6$), it normally indicates that the Pt tip is in the hydrogen diffusion layer and further approach to the substrate may crash the Pt tip. As such, the position for $I/I_\infty \approx 0.6$ was used to obtain the final tip−substrate distance, which was determined to be about 5 μm for V-MoS_2 and 4 μm for SV-MoS_2. Once the tip was positioned at the set distances over the MoS_2 substrates, the MoS_2 substrates were electrochemically activated and stabilized by cycling between 0 V and −0.5 V in 0.1 M $HClO_4$ at a scan rate of 20 mV/s for about five cycles. After stabilization, the LSV measurements were performed by sweeping the applied potential on MoS_2 from 0 V to −0.7 V at a scan rate of 5 mV/s to generate H_2 while holding the Pt UME tip potential at 0 V to oxidize the generated H_2 into protons.

Figure 3 shows representative SECM LSV plots of the Pt tip current (Figure 3a) and substrate current (Figure 3b) for which the substrate is the unstrained MoS_2 monolayer with S vacancies (V-MoS_2). The abrupt decrease in tip current at −0.68 V in Figure 3a was caused by the formation of hydrogen bubbles, which crossed the tip−substrate gap and made contact with the Pt UME. The overall current collection efficiency, that is, the ratio between the tip current and the substrate current, is small at about 1.37%, which is reasonable because the tip size is much smaller than the size of the substrate. To obtain the HER kinetic parameters for the V-MoS_2 substrate, 2-D axial symmetric COMSOL simulations were carried out to calculate the time-dependent H^+ (with concentration C_O) and H_2 (with concentration C_R) distribution (Figure 1b; see Supporting Information for details).[34,35] For the simulation, the forward (K_{fv}) and backward (K_{bv}) HER reaction rates on the V-MoS_2 working electrode were calculated using the following equations:

$$K_{fv} = k_v^0 \times e^{[-\alpha_v nf(E_{sub}-E_v^0)]}$$

$$K_{bv} = k_v^0 \times e^{[(1-\alpha_v)nf(E_{sub}-E_v^0)]}$$

where $f = F/RT$ [~38.92/V, given Faraday's constant $F = 9.6 \times 10^4$ C/mol, the ideal gas constant R = 8.3 J/(K·mol), and temperature T = 298 K] and E_v^0, α_v, and k_v^0 are the corresponding formal potential, electron-transfer coefficient, and electron-transfer rate constant to be determined. For the HOR on the Pt tip, its forward and backward reaction rates were calculated using the reported electron-transfer kinetic parameters of E_t^0 = −0.40 V, α_t = 0.5, and k_t^0 = 0.42 cm/s.[13,34] Since the SECM operated in the diffusion-controlled regime, the calculated C_O and C_R profiles were then used to calculate the substrate HER and Pt tip HOR current by using Fick's first law of diffusion:

$$\frac{i_{HER}}{nFA} = D_O\frac{\partial C_O}{\partial z}, \quad \frac{i_{HOR}}{nFA} = D_R\frac{\partial C_R}{\partial z}$$

where i is the current, n is the electron number, A is the electrode area, and D_O and D_R are the proton and H_2 diffusion coefficients, respectively.[34,35] By identifying the best fit between

DOI: 10.1021/jacs.6b01377
J. Am. Chem. Soc. 2016, 138, 5123−5129

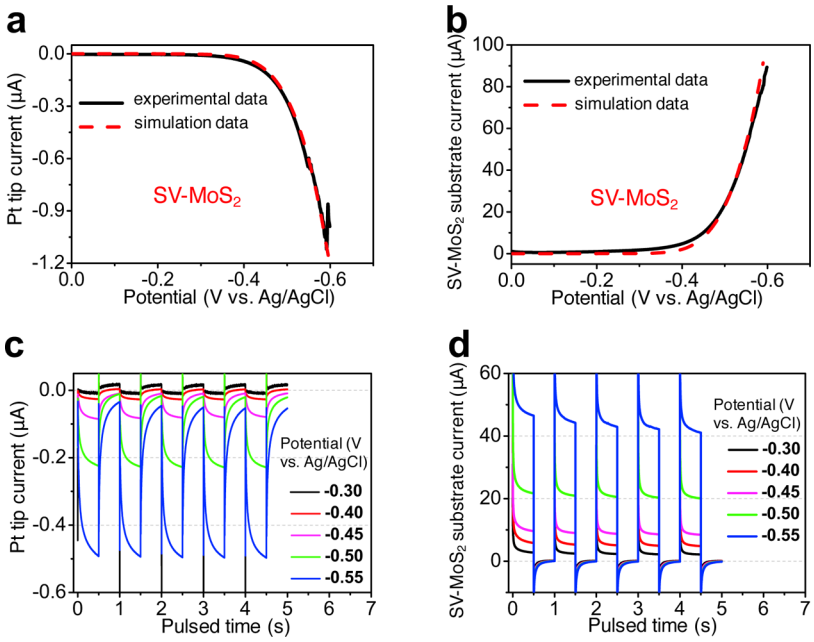

Figure 4. Experimental SECM measurement results of SV-MoS_2 and the corresponding simulation results. (a) Pt tip and (b) SV-MoS_2 substrate voltammograms in 0.1 M $HClO_4$ electrolyte and the corresponding simulation results (red dashed lines). The separation between the tip and substrate electrode was ~4 μm. Tip potential was held at 0 V, and the substrate potential was swept from 0 V to −0.6 V at a scan rate of 5 mV/s. Transient and oscillating (c) Pt tip and (d) SV-MoS_2 substrate current according to the double-pulse potential applied to the substrate. Tip potential was held at 0 V, and the substrate potential was switched between open circuit potential and the potentials listed in the legend to enable MoS_2 for HER. The pulse width was 0.5 s with five replicates.

the calculated currents (Figure 3a,b, dashed lines) and the measured currents (Figure 3a,b, solid lines), the HER kinetic data (E_v^0 = −0.53 V, α_v = 0.4, k_v^0 = 2.3 × 10^{-4} cm/s) were determined for V-MoS_2.

Since the HER would not reach the steady state in 0.1 M $HClO_4$ acid during our SECM measurement, we further conducted transient response measurements to verify the above kinetic parameters extracted from the LSV curves. For the transient response study,[36] we applied a pulse potential to the MoS_2 substrate electrode between the OCP and various negative potentials with a pulse width of 0.5 s for five replicates. The applied potential to the Pt tip was held at 0 V, which was much more positive than the HOR formal potential (−0.40 V), so that the HOR proceeded at a diffusion-controlled rate on the Pt tip, which ensured the validity of extracting the HER kinetic parameters from the tip current, as discussed earlier. The corresponding transient Pt tip and MoS_2 substrate currents are plotted in Figure 3c,d, respectively, and both show similar oscillating behavior. First, the Pt tip current (Figure 3c) is nearly 0 A when a MoS_2 substrate is at the OCP (without any HER activity), which shows no hysteresis for H_2 collection on the Pt tip. Second, when more negative potential is applied to MoS_2, it generates a larger HER substrate current and larger Pt tip HOR current, which verifies that the Pt tip HOR current is indeed controlled by the H_2 diffusion flux. Moreover, it is noted that both the tip and the V-MoS_2 substrate currents agree with the electron-transfer kinetics obtained from Figure 3a,b, which also suggests that the one-electron reaction model with a Butler−Volmer equation provides a reasonable formalism to treat the complex HER kinetics on V-MoS_2.

Next, we applied similar SECM measurement steps (as discussed above for V-MoS_2) to the SV-MoS_2 sample with a current collection efficiency of ~1.26%. The corresponding kinetic data for SV-MoS_2 were determined to be E_{sv}^0 = −0.53 V, α_{sv} = 0.4, and k_{sv}^0 = 1.0 × 10^{-3} cm/s by best fit of the calculated currents (Figure 4a,b, dashed lines) with the measured currents (Figure 4a,b, solid lines). It is noted that the sudden decrease in tip current at −0.6 V in Figure 4a was also caused by hydrogen bubble formation and accumulation, similar to that shown in Figure 3a. The accuracy of our extracted kinetic information is also supported by a similar transient tip and substrate current measurements, as shown in Figure 4c,d. The comparisons of those tip and substrate currents for the V-MoS_2 and SV-MoS_2 substrates are shown in Figure S4a−d, which clearly show that the onset potential for SV-MoS_2 is about 0.1 V more positive than that of the V-MoS_2, and the HER current of the SV-MoS_2 is about 4 times larger than that of V-MoS_2 at the same potential of −0.55 V. Those comparisons are consistent with the previous observation that tensile strain further enhances the HER activity of the S vacancies.[11] The enhancement effect on HER by strain is more evidenced by comparing the extracted kinetic data, as summarized in Table 1. Though V-MoS_2 and SV-MoS_2 have similar formal potential E^0 (−0.53 V) and electron-transfer coefficient α (0.4), the electron-transfer rate

Table 1. Extracted Kinetic Parameters for HER over V-MoS_2 and SV-MoS_2[a]

kinetic parameters	unstrained MoS_2 with S vacancies (V-MoS_2)	strained MoS_2 with S vacancies (SV-MoS_2)
E^0 (V vs Ag/AgCl)	−0.53	−0.53
a	0.4	0.4
k^0 (cm/s)	2.3 × 10^{-4}	1.0 × 10^{-3}

[a]Other parameters used for fitting: proton diffusion coefficient of 7.9 × 10^{-5} cm^2/s, hydrogen diffusion coefficient of 5 × 10^{-5} cm^2/s, and proton concentration of 0.1 M.

DOI: 10.1021/jacs.6b01377
J. Am. Chem. Soc. 2016, 138, 5123−5129

constant k^0 for SV-MoS_2 is about 4 times higher than that of V-MoS_2.

Finally, the reliability of our SECM measurement was confirmed by four more repeated measurements of the V-MoS_2 and SV-MoS_2 regions on the same substrate (Figure S5, where the error bars represent the standard deviation). The very small errors suggest that our SECM measurements are reliable. We further confirmed this by complementary measurements using a three-electrode electrochemical compression cell that has a diameter of 3 mm (see our previous work for more details[11]). The average LSV ranges of both V-MoS_2 and SV-MoS_2 samples (eight samples total) are represented by shaded regions in Figure S6. One can see that the separate measurements agree reasonably well despite the different electrolytes and sample dimensions of the two distinct measurements.

CONCLUSION

In summary, we have successfully applied the combinational approach of SECM measurements and multiphysics modeling to investigate the HER kinetics of newly identified active sites that consist of S vacancies on the basal plane of MoS_2. The HER kinetic data for S vacancies were determined to be the formal potential $E_v^0 = -0.53\ V_{Ag/AgCl}$, electron-transfer coefficient $\alpha_v = 0.4$, and electron-transfer rate constant $k_v^0 = 2.3 \times 10^{-4}$ cm/s. In addition, the effect of tensile strain on the HER kinetics of S vacancies was quantified. About 2% uniaxial tensile strain increases the electron-transfer rate constant by almost 4-fold ($k_{sv}^0 = 1.0 \times 10^{-3}$ cm/s), confirming that the tensile elastic strain indeed accelerates the HER kinetics of S vacancies in MoS_2. The methodology presented here provides a general way to study the electrochemical kinetics of MoS_2-like two-dimensional catalytic systems.

ASSOCIATED CONTENT

Supporting Information

The Supporting Information is available free of charge on the ACS Publications website at DOI: 10.1021/jacs.6b01377.

Supporting figures of the Raman spectra of strained and unstrained MoS_2, optical image of a typical SECM sample, schematic SECM measurement setup, measured and calculated SECM approach curves, comparison of HER activities of V-MoS_2 and SV-MoS_2, comparison of LSV curves of Pt, V-MoS_2, and SV-MoS_2, complementary LSV measurements using an electrochemical compression cell, simulated LSV curves at various k^0; Supporting Note 1 of sample fabrication and characterization; Supporting Note 2 of substrate electrode preparation, Pt UME tip preparation, and SECM measurements; Supporting Note 3 of multiphysics simulation (PDF)

AUTHOR INFORMATION

Corresponding Authors

*ajbard@cm.utexas.edu
*xlzheng@stanford.edu

Author Contributions

¶H.L. and M.D. contributed equally to this work.

Notes

The authors declare no competing financial interest.

ACKNOWLEDGMENTS

This work was financially supported by the National Science Foundation (CHE-1405248), and the 2013 Global Research Outreach (GRO) Program (Award No. IC2012-1318) of the Samsung Advanced Institute of Technology (SAIT) and Samsung R&D Center America, Silicon Valley (SRA-SV), under the supervision of Dr. Debasis Bera and Anthony Radspieler, Jr. Part of this work was performed at the Stanford Nano Shared Facilities (SNSF).

REFERENCES

(1) Nidola, A.; Schira, R. *Int. J. Hydrogen Energy* **1986**, *11*, 449−454.
(2) Merki, D.; Hu, X. *Energy Environ. Sci.* **2011**, *4*, 3878−3888.
(3) Laursen, A. B.; Kegnaes, S.; Dahl, S.; Chorkendorff, I. *Energy Environ. Sci.* **2012**, *5*, 5577−5591.
(4) Benck, J. D.; Hellstern, T. R.; Kibsgaard, J.; Chakthranont, P.; Jaramillo, T. F. *ACS Catal.* **2014**, *4*, 3957−3971.
(5) Hinnemann, B.; Moses, P. G.; Bonde, J.; Jørgensen, K. P.; Nielsen, J. H.; Horch, S.; Chorkendorff, I.; Nørskov, J. K. *J. Am. Chem. Soc.* **2005**, *127*, 5308−5309.
(6) Jaramillo, T. F.; Jørgensen, K. P.; Bonde, J.; Nielsen, J. H.; Horch, S.; Chorkendorff, I. *Science* **2007**, *317*, 100−102.
(7) Chen, Z.; Cummins, D.; Reinecke, B. N.; Clark, E.; Sunkara, M. K.; Jaramillo, T. F. *Nano Lett.* **2011**, *11*, 4168−4175.
(8) Kibsgaard, J.; Chen, Z.; Reinecke, B. N.; Jaramillo, T. F. *Nat. Mater.* **2012**, *11*, 963−969.
(9) Kong, D.; Wang, H.; Cha, J. J.; Pasta, M.; Koski, K. J.; Yao, J.; Cui, Y. *Nano Lett.* **2013**, *13*, 1341−1347.
(10) Ataca, C.; Ciraci, S. *Phys. Rev. B: Condens. Matter Mater. Phys.* **2012**, *85*, 195410.
(11) Li, H.; Tsai, C.; Koh, A. L.; Cai, L.; Contryman, A. W.; Fragapane, A. H.; Zhao, J.; Han, H. S.; Manoharan, H. C.; Abild-Pedersen, F.; Nørskov, J. K.; Zheng, X. *Nat. Mater.* **2016**, *15*, 48−53.
(12) Bard, A. J.; Fan, F. R. F.; Kwak, J.; Lev, O. *Anal. Chem.* **1989**, *61*, 132−138.
(13) Zhou, J.; Zu, Y.; Bard, A. J. *J. Electroanal. Chem.* **2000**, *491*, 22−29.
(14) Leonard, K. C.; Bard, A. J. *J. Am. Chem. Soc.* **2013**, *135*, 15890−15896.
(15) Bonazza, H. L.; Vega, L. D.; Fernández, J. L. *J. Electroanal. Chem.* **2014**, *713*, 9−16.
(16) Ahmed, S.; Ji, S.; Petrik, L.; Linkov, V. M. *Anal. Sci.* **2004**, *20*, 1283−1287.
(17) Li, F.; Ciani, I.; Bertoncello, P.; Unwin, P. R.; Zhao, J.; Bradbury, C. R.; Fermin, D. J. *J. Phys. Chem. C* **2008**, *112*, 9686−9694.
(18) Li, F.; Bertoncello, P.; Ciani, I.; Mantovani, G.; Unwin, P. R. *Adv. Funct. Mater.* **2008**, *18*, 1685−1693.
(19) Fernández, J. L. *J. Electroanal. Chem.* **2010**, *650*, 90−97.
(20) Bertoncello, P. *Energy Environ. Sci.* **2010**, *3*, 1620−1633.
(21) Lai, S. C. S.; Macpherson, J. V.; Unwin, P. R. *MRS Bull.* **2012**, *37*, 668−674.
(22) Wain, A. J. *Electrochem. Commun.* **2014**, *46*, 9−12.
(23) Li, H.; Contryman, A. W.; Qian, X.; Ardakani, S. M.; Gong, Y.; Wang, X.; Weisse, J. M.; Lee, C. H.; Zhao, J.; Ajayan, P. M.; Li, J.; Manoharan, H. C.; Zheng, X. *Nat. Commun.* **2015**, *6*, 7381.
(24) Ma, Q.; Odenthal, P. M.; Mann, J.; Le, D.; Wang, C. S.; Zhu, Y.; Chen, T.; Sun, D.; Yamaguchi, K.; Tran, T.; Wurch, M.; McKinley, J. L.; Wyrick, J.; Magnone, K.; Heinz, T. F.; Rahman, T. S.; Kawakami, R.; Bartels, L. *J. Phys.: Condens. Matter* **2013**, *25*, 252201.
(25) Rice, C.; Young, R. J.; Zan, R.; Bangert, U.; Wolverson, D.; Georgiou, T.; Jalil, R.; Novoselov, K. S. *Phys. Rev. B: Condens. Matter Mater. Phys.* **2013**, *87*, 081307.
(26) Jia, C. L.; Urban, K. *Science* **2004**, *303*, 2001−2004.
(27) Urban, K. W. *Science* **2008**, *321*, 506−510.
(28) Martin, R. D.; Unwin, P. R. *Anal. Chem.* **1998**, *70*, 276−284.
(29) Sanchez-Sanchez, C. M.; Rodriguez-Lopez, J.; Bard, A. J. *Anal. Chem.* **2008**, *80*, 3254−3260.

DOI: 10.1021/jacs.6b01377
J. Am. Chem. Soc. 2016, 138, 5123−5129

(30) Li, H.; Zhang, Q.; Yap, C. C. R.; Tay, B. K.; Teo, H. T. E.; Olivier, A.; Baillargeat, D. *Adv. Funct. Mater.* **2012**, *22*, 1385−1390.
(31) Unwin, P. R.; Bard, A. J. *J. Phys. Chem.* **1991**, *95*, 7814−7824.
(32) Kwak, J.; Bard, A. J. *Anal. Chem.* **1989**, *61*, 1221−1227.
(33) Bard, A. J.; Denuault, G.; Lee, C.; Mandler, D.; Wipf, D. O. *Acc. Chem. Res.* **1990**, *23*, 357−363.
(34) Zoski, C. G. *J. Phys. Chem. B* **2003**, *107*, 6401−6405.
(35) Sheng, W.; Gasteiger, H. A.; Shao-Horn, Y. *J. Electrochem. Soc.* **2010**, *157*, B1529−B1536.
(36) Minguzzi, A.; Battistel, D.; Rodríguez-López, J.; Vertova, A.; Rondinini, S.; Bard, A. J.; Daniele, S. *J. Phys. Chem. C* **2015**, *119*, 2941−2947.

DOI: 10.1021/jacs.6b01377
J. Am. Chem. Soc. 2016, 138, 5123−5129